The background of the slide is composed of numerous overlapping, 3D-style cones. The cones are colored in two shades: cyan and light green. They are arranged in a dense, somewhat chaotic pattern, with some pointing upwards and others downwards, creating a textured, forest-like appearance. The text is centered over this background.

# **Cosmography And Radio Pulsar Experiment**

Judd D. Bowman  
October 10, 2009

# CARPE collaboration

Judd Bowman (Caltech)

Rich Bradley (NRAO/UVA)

Jacqueline Hewitt (MIT)

David Kaplan (UCSB/Milwaukee)

Avi Loeb (Harvard)

Maura McLaughlin (WVU)

Miguel Morales (U. Washington)

Stuart Wyithe (Melbourne)

## Students:

Eli Visbal (Harvard)

Paul Geil (Melbourne)

Alex Fry (U. Washington)

Christian Boutan (U. Washington)

# Outline

1. Overview and motivation
2. Reference antenna concept
3. Performance
  
4. Sites and RFI
5. Foreground subtraction

# Dark energy

- $1 < z < 4$ : beneficial for models poorly described by  $w$  and  $w'$  at  $z=1$
- Transverse and line-of-sight BAO scales: [spectroscopic and photometric galaxy surveys are mostly sensitive to transverse](#)
- 2D BAO spectrum gives better constraints than spherically binned
- Sensitive to only dark matter power spectrum and four additional parameters:
  - Mass weighted neutral hydrogen fraction  $x_{\text{HI}}$
  - HI mass weighted halo bias  $\langle b \rangle$
  - Ionizing photon mean free path  $k_{\text{mfp}}$
  - Fluctuations in the ionizing background  $K_0$  (<1% suppression on large scales since UV field is nearly uniform after reionization )
- Robust against non-linear effects in the linear and quasi-linear regimes

# Pulsars

## Searches

- Local sources at low luminosities at lower frequencies
- Distant brighter objects at higher frequencies
- Deep searches of the Magellanic clouds in single pointings
- Repeated survey the entire sky: [sporadic sources](#), [intermittent sources](#), [rapidly precessing systems \(e.g. binaries\)](#)
- Better RFI rejection with many beams

## Timing

- Dedicated observations: [probe emission physics](#), [establish orbital parameters](#), and [test gravity](#)
- Multiple pulsars timed simultaneously: [refine pulsar ephemerides](#), [remove systematics effects](#), [improving gravitational wave studies](#)

# Approach

1. Dark Energy IM is exactly same problem as reionization
2. Leverage existing MWA, LOFAR, PAPER efforts
3. To minimize risk and development overhead:
  - Design a Dark Energy array that closely builds on low-frequency heritage
  - Incorporate lessons learned on [foreground subtraction](#) and [calibration](#)
4. Be ready to start construction as soon as reionization arrays prove technique is successful

# The MWA as an example



# The MWA as an example



# The MWA as an example



Saturday, October 10, 2009

# CARPE reference design

Number of antennas:	2500 (steerable)
Antenna effective area:	1.28 - 5.14 m <sup>2</sup>
Total collecting area:	3000 - 12,500 m <sup>2</sup>
Field of view:	~20 deg
Available bands:	high: 0.2 - 0.5 m (600-1500 MHz) low: 0.4 - 1.0 m (300-700 MHz)
Redshift range:	$0 < z < 4$
Instantaneous bandwidth:	300 MHz
Maximum baseline:	250 m
Angular resolution:	3 to 11 arcmin
MOFF dimension:	512 x 512
Observing strategy:	3 fields, each for 2000 hours per year (2x more efficient than drifting)
Target cost:	\$50M

# Sensitivity scaling laws

	$A _{dA}$	$A _{N_A}$	$dA _A$	$B$	$k$	$t$
Power Spec. S/N	$A^2$	$A^{3/2}$	$(dA)^{-1/2} \propto \text{FOV}$	$B^{1/2}$	$k \bar{n}(k)$	$t$

Table 2: Approximate scaling relationships for the power spectrum signal-to-noise ratio (excerpted from Morales (2005)). In order, the scalings in each column are: total array area holding the size of each antenna constant  $A|_{dA}$  (adding antennas), total array area holding the number of antennas and distribution constant  $A|_{N_A}$  (increasing antenna size), the size of each antenna with the total array area held constant  $dA|_A$  (dividing area into more small antennas), the total bandwidth  $B$ , the sensitivity as a function of wavenumber length  $k$  where  $\bar{n}(k)$  is the density of baselines (average of  $u, v$  coverage as function of wavenumber), and the total observing time  $t$ .

# FOV and resolution requirements

$z = 1$ :

150 Mpc

$> 2.5$  deg

$> 25$  MHz

8 Mpc

$< 4$  arcmin

$< 1$  MHz

$z = 4$ :

150 Mpc

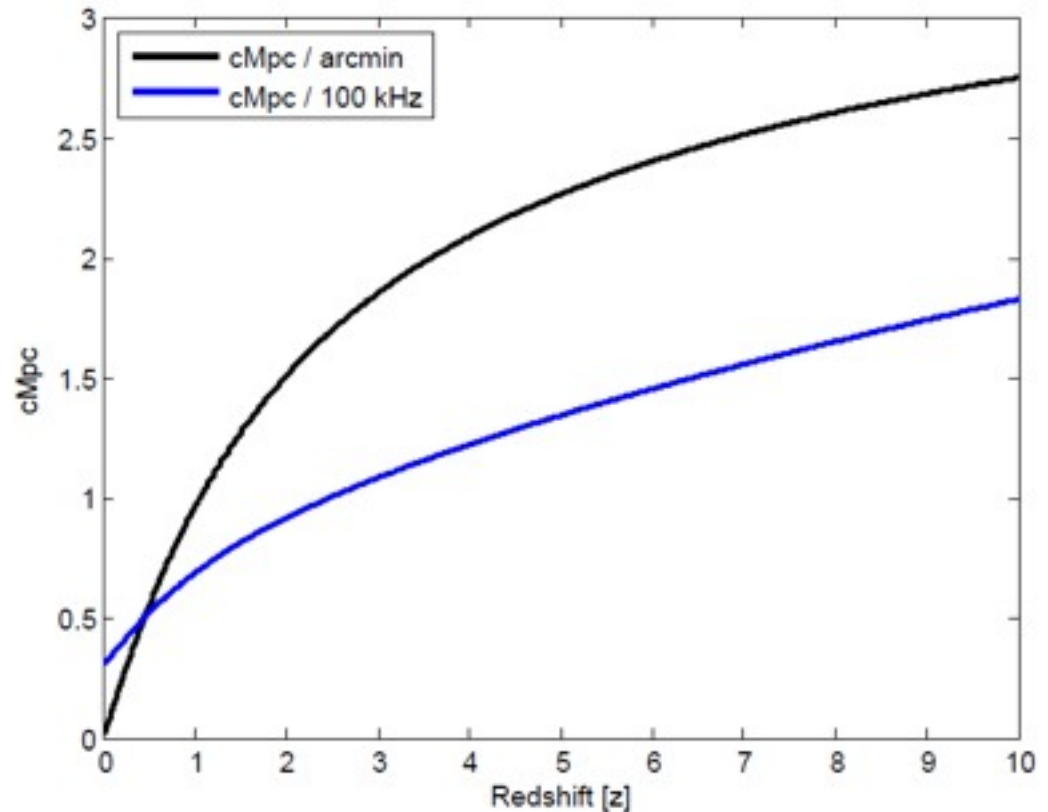
$> 1.5$  deg

$> 15$  MHz

8 Mpc

$< 2$  arcmin

$< 0.5$  MHz



Largest angular scale retained = largest spectral scale after foreground subtraction

# CARPE reference design



Saturday, October 10, 2009

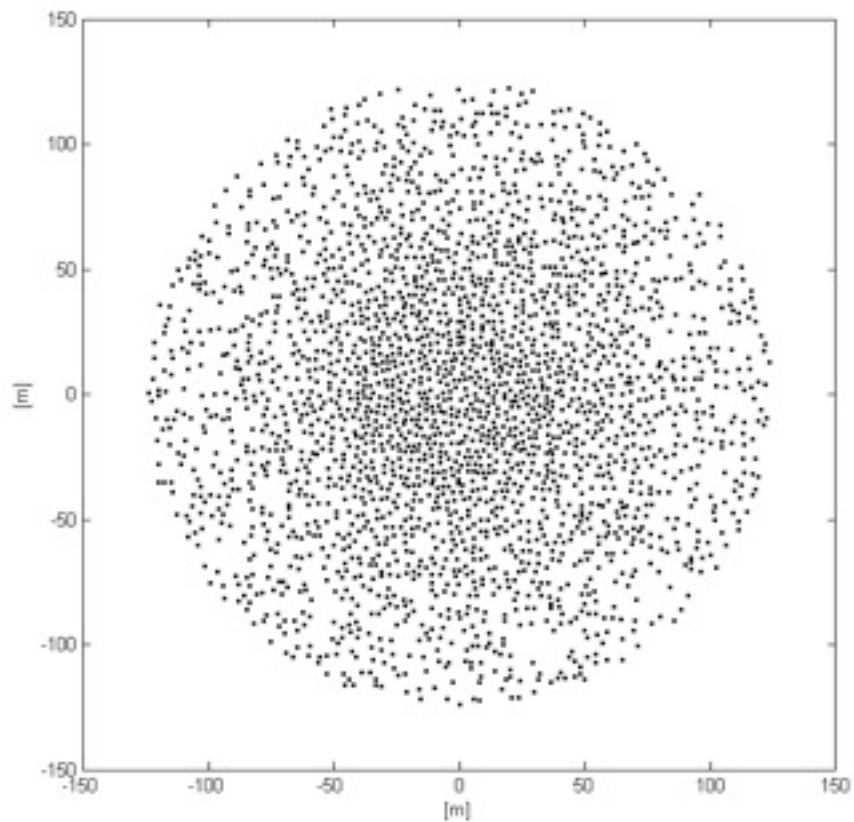
# CARPE reference design



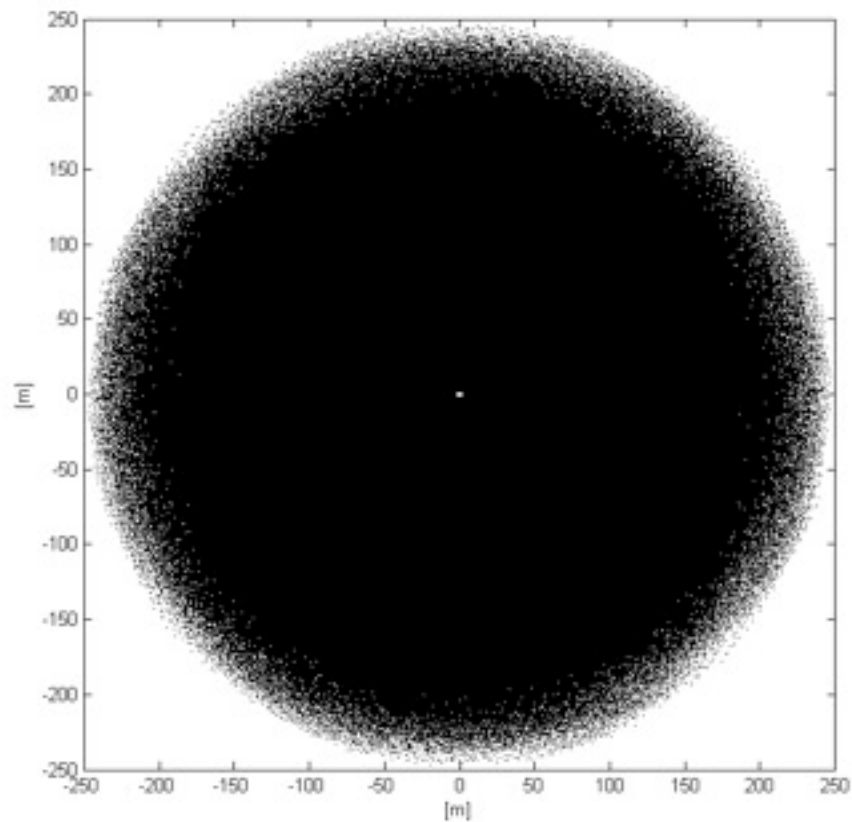
Saturday, October 10, 2009

# Instantaneous UV coverage

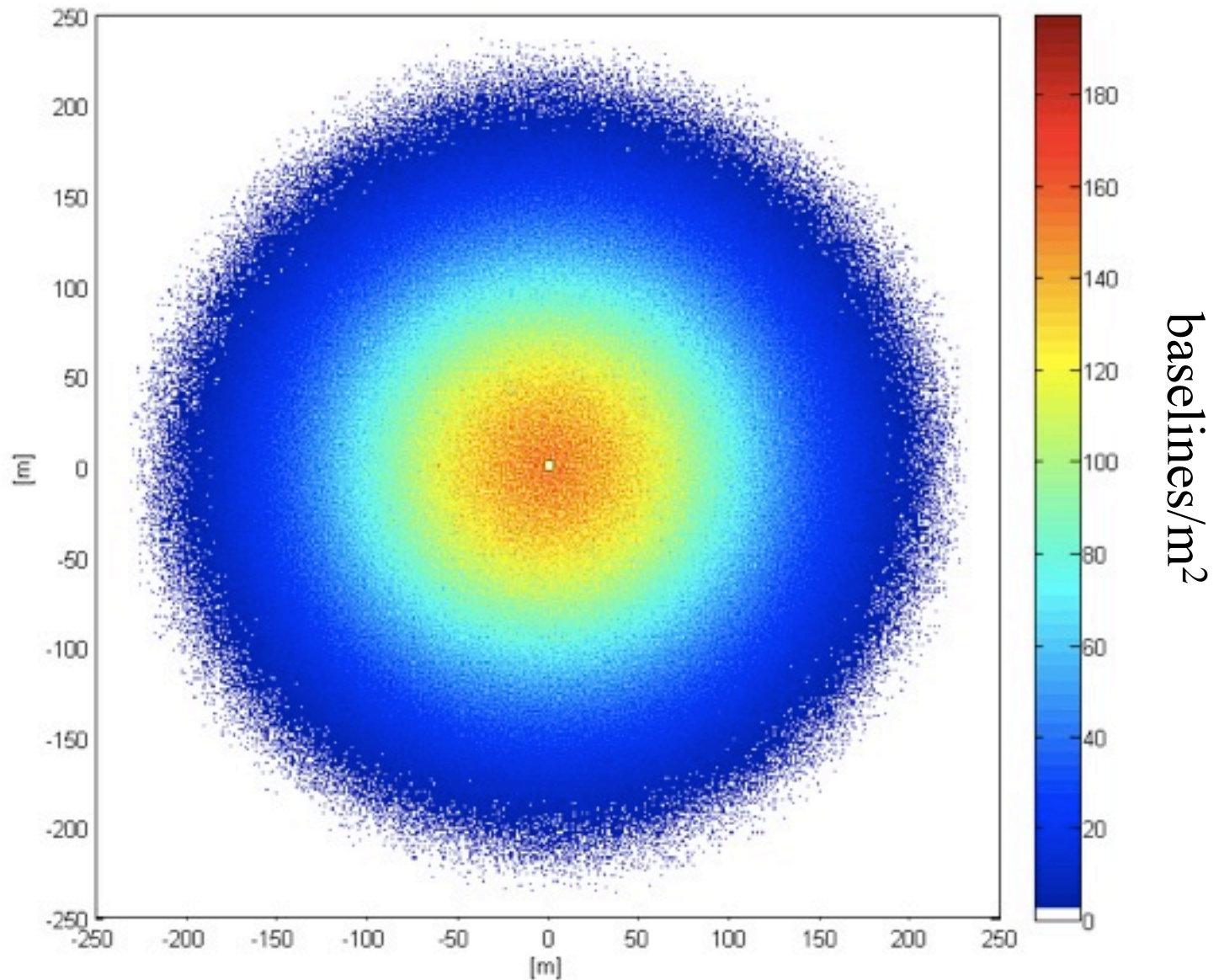
## Antennas



## Baselines



# Instantaneous UV redundancy



# Point source (mis-)subtraction

- Must localize sources to 0.1" for MWA
  - Scales with number of antennas, so close to  $\sim 1''$  for CARPE
  - Only 0.5% of beam, so need  $\text{SNR} \sim 200$

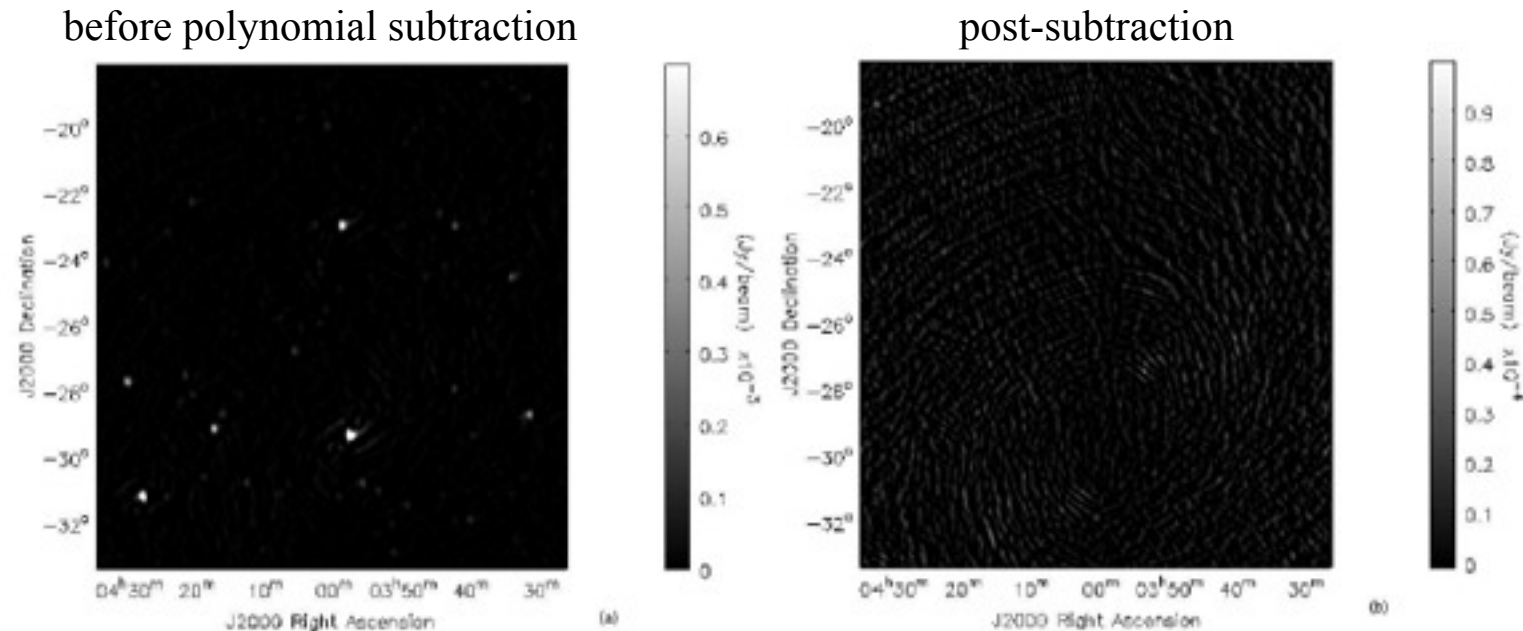


FIG. 5.— (a) Dirty UVSUBed image of the field made from  $V_{ij}^{\text{obs}}$  after the imperfect GSM ( $V_{ij}^{\text{GSM}_{\text{imperfect}}}$ ) has been subtracted from the perfect data-set ( $V_{ij}^{\text{obs}}$ ). (b) The image of the field after the IMLIN has been applied to the UVSUBed image in figure a.

# Calibration error limits

- MWA residual calibration errors should be  $\sim 0.01\%$  in amplitude or  $\sim 0.01$  degree in phase at *end of integration*
  - Scales with number of antennas, 5x easier for CARPE
  - 0.2% in amplitude and 0.2 degree in phase per day

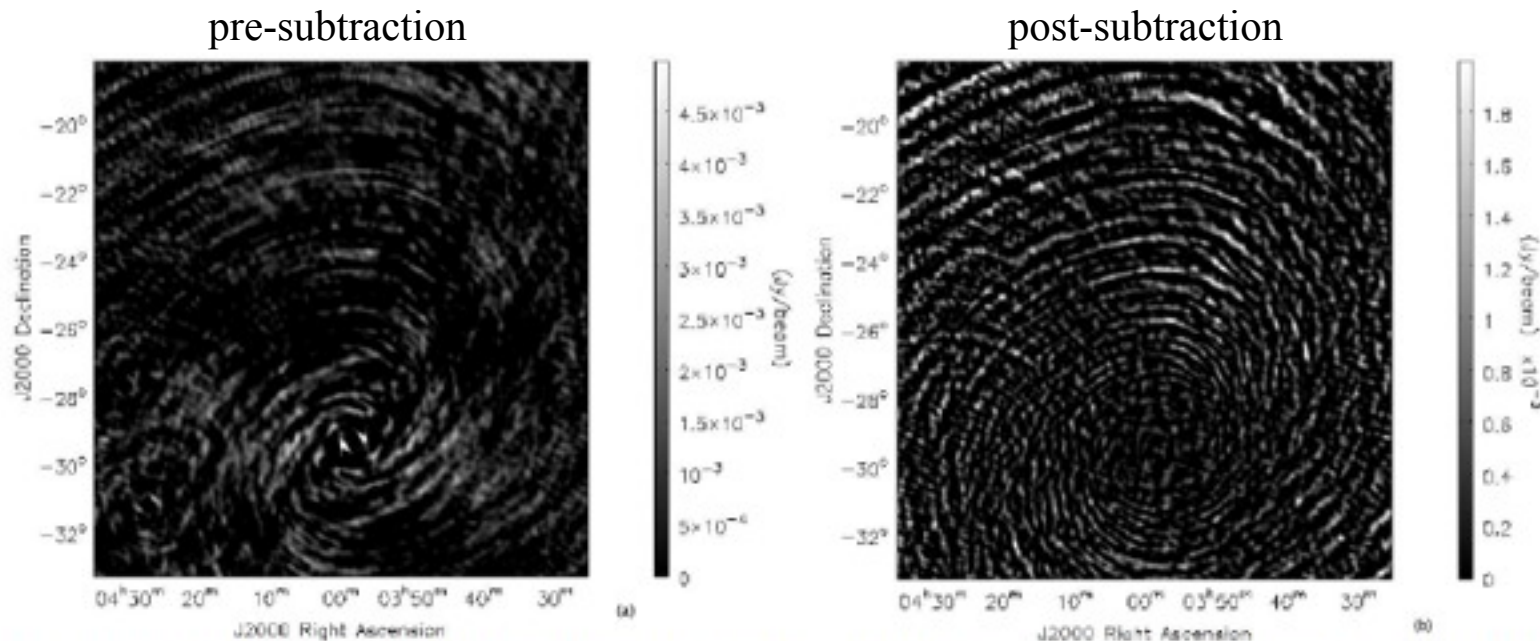


FIG. 7.— (a) Dirty UVSUBed image of the field made from the  $V_{ij}^{\text{obs}}$ , after the model visibilities corrupted with residual calibration errors ( $V_{ij}^{\text{corr}}$ ) has been subtracted from the perfect data-set ( $V_{ij}^{\text{obs}}$ ). (b) The image of the field after the IMLIN has been applied to the UVSUBed image in figure a.

# Key technologies

1. MOFF correlator
2. Inexpensive broadband antennas
3. Precision calibration techniques from reionization arrays

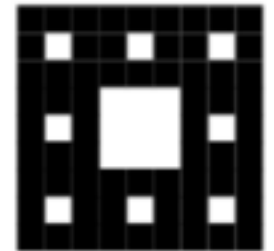
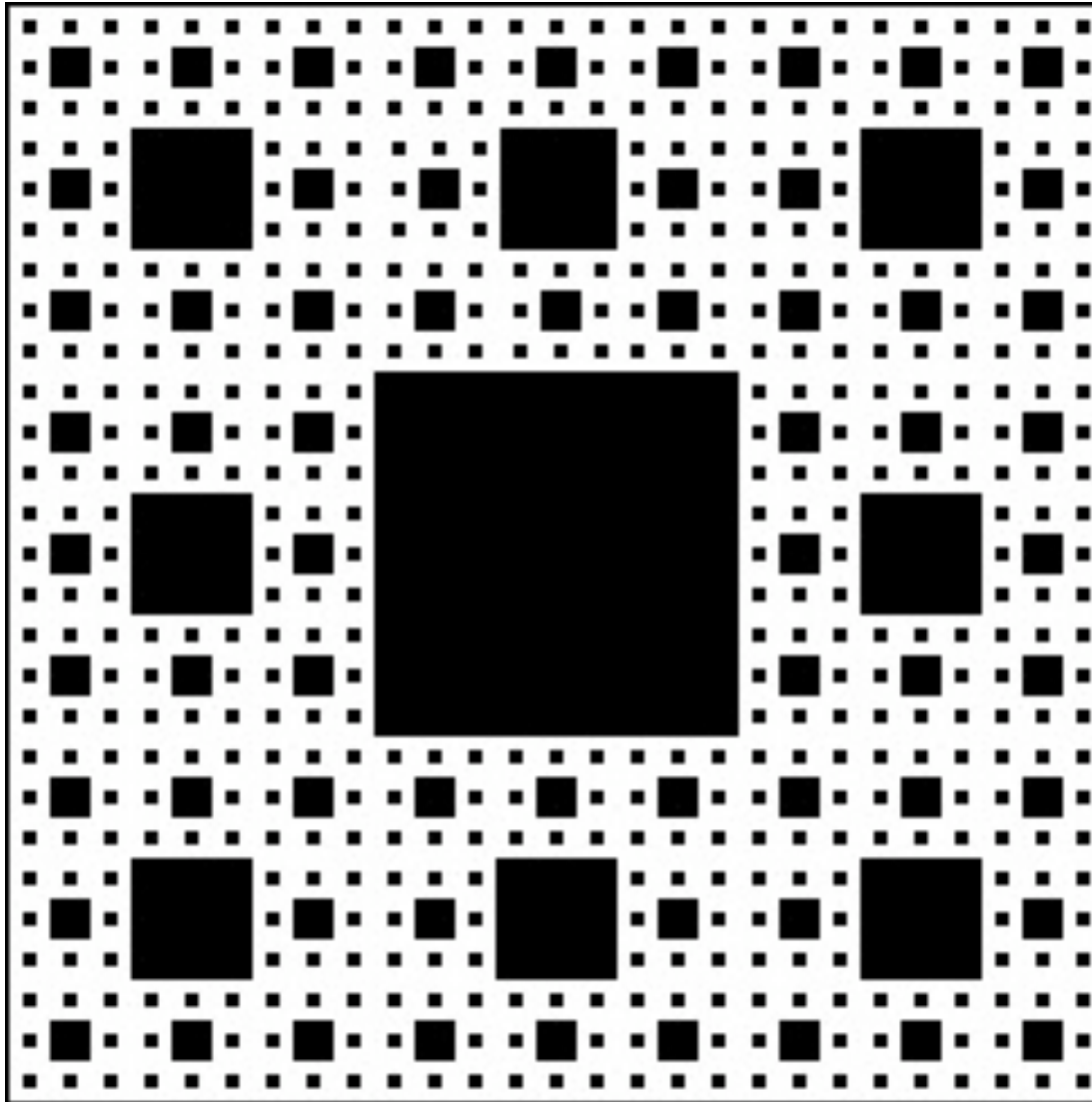
# MOFF

- Output image has the equivalent information of the FX correlator visibilities, allowing precision deconvolution and polarimetry.
- Antennas do not need to be placed on a regular grid.
- Computationally efficient for compact arrays with a high spatial density of antennas: CARPE MOFF correlator is 14 times more efficient than FX (2.7e14 CMAC/s compared to 3.7e15 CMAC/s for FX)
- MOFF correlation depends on the physical size of the array and not the number of antennas: easily scale to  $\sim 10000$  antennas with fractional increase in computational load
- A fully calibrated electric field image is created as an intermediate product. The number of calibrated pulsar beams available is limited only by the output bandwidth, and hardware de-dispersion can be easily incorporated.

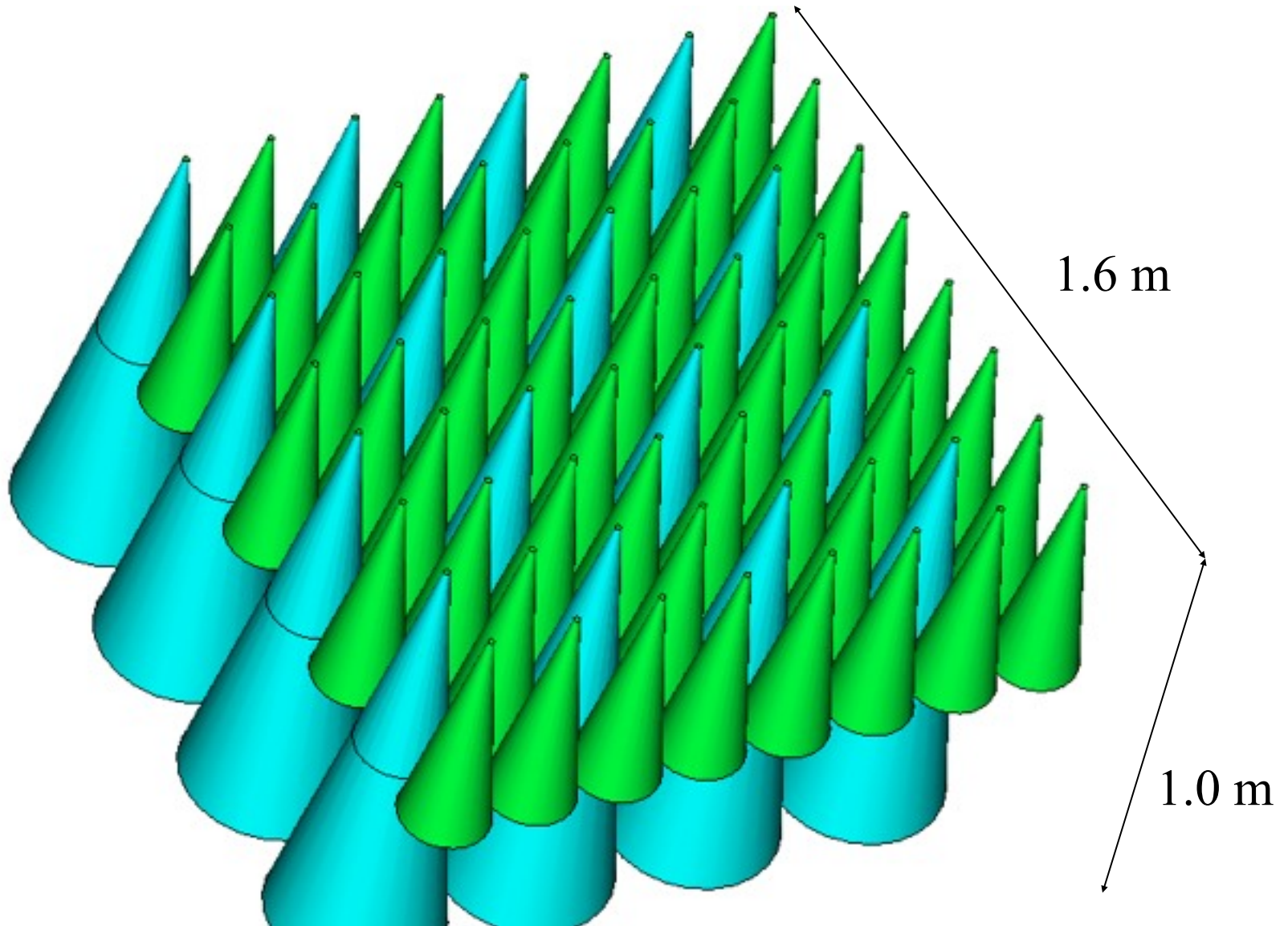
# CARPE Antenna Concept

Richard Bradley (NRAO/UVA)

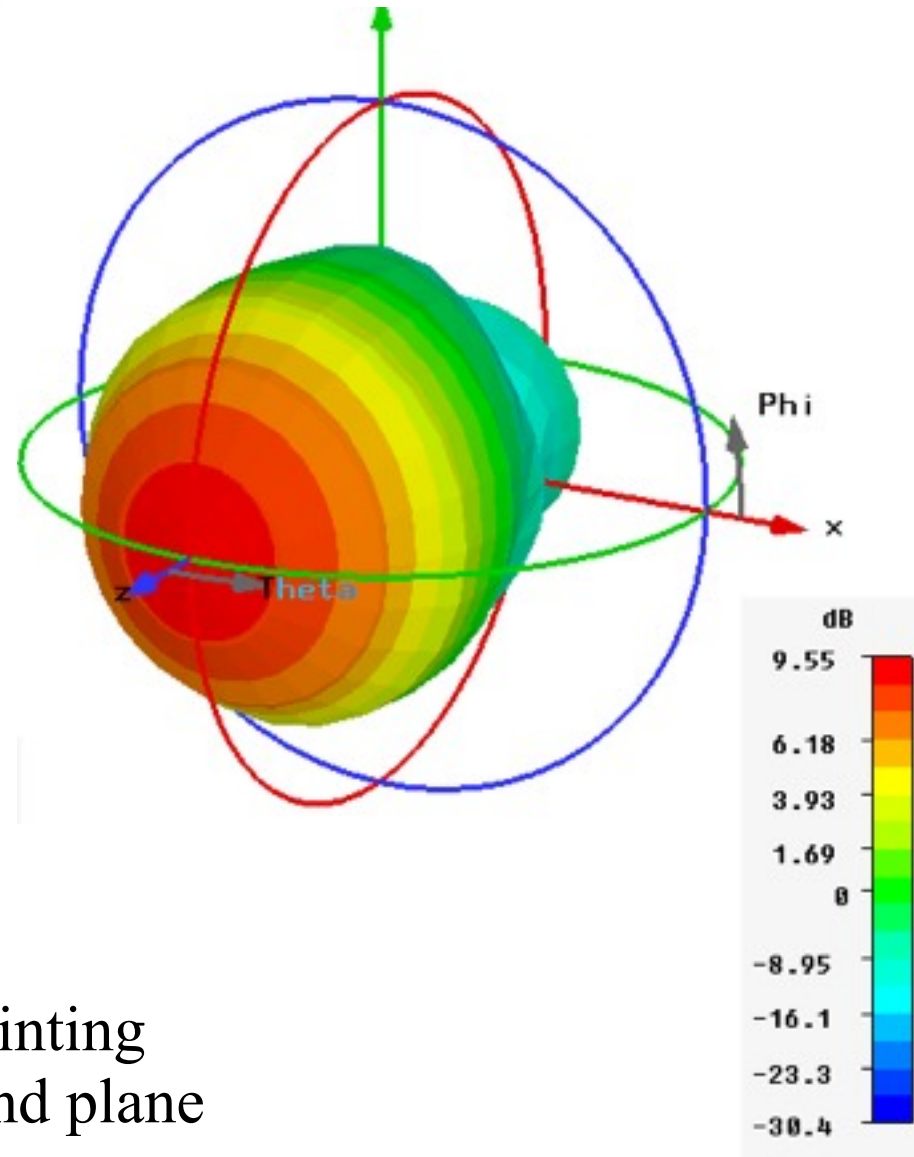
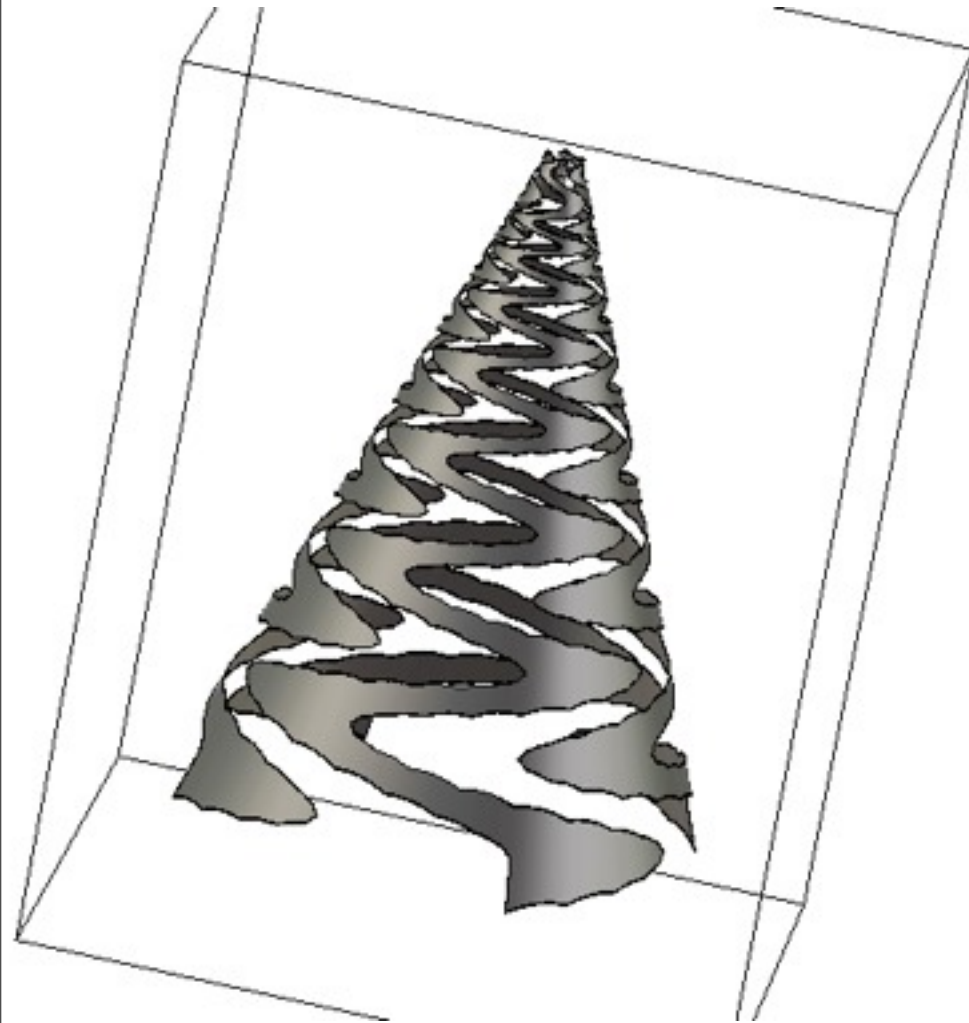
# Sierpinski carpet fractal



# Dual level: 4x4 low – 8x8 high

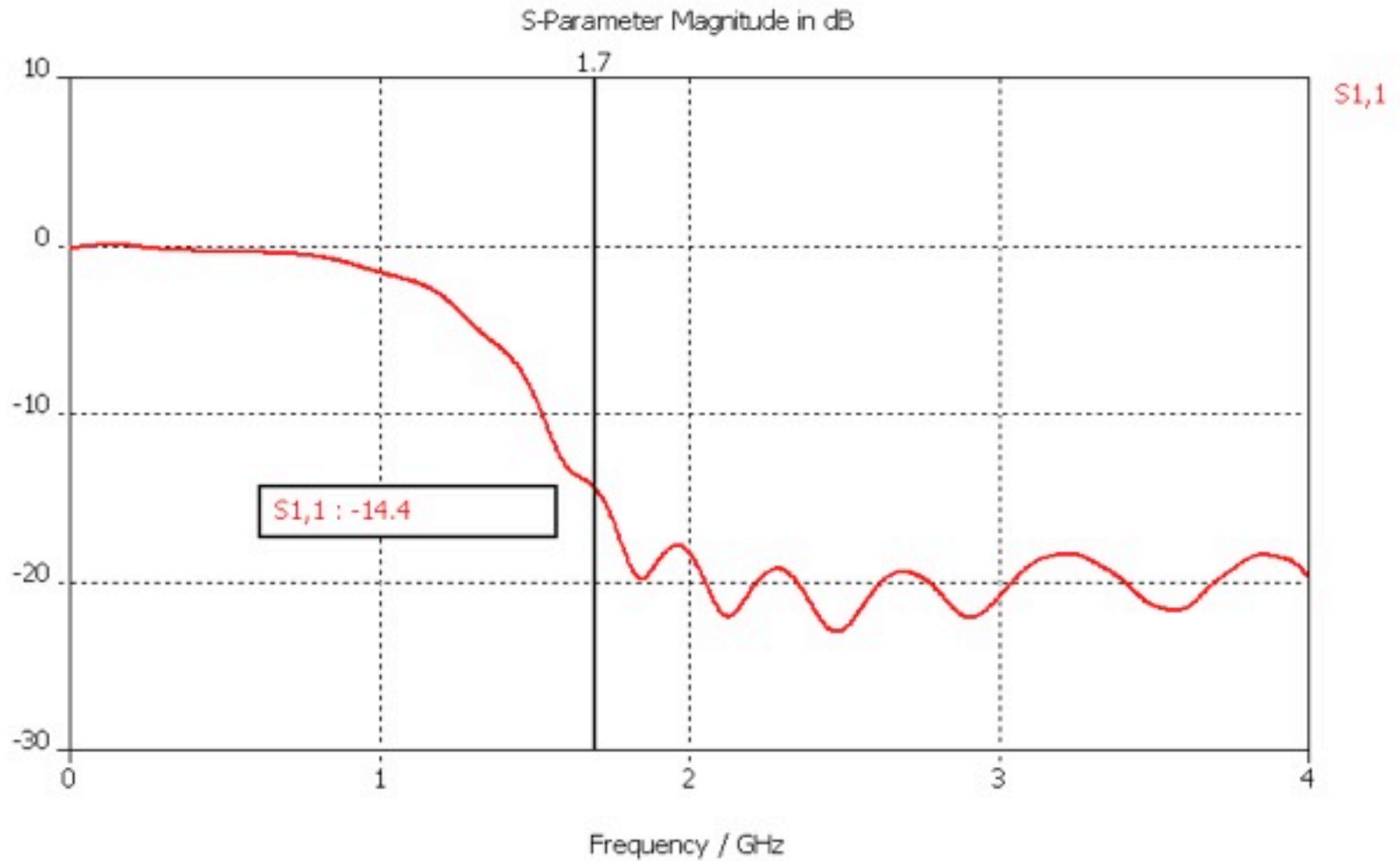


# Sinuuous cone

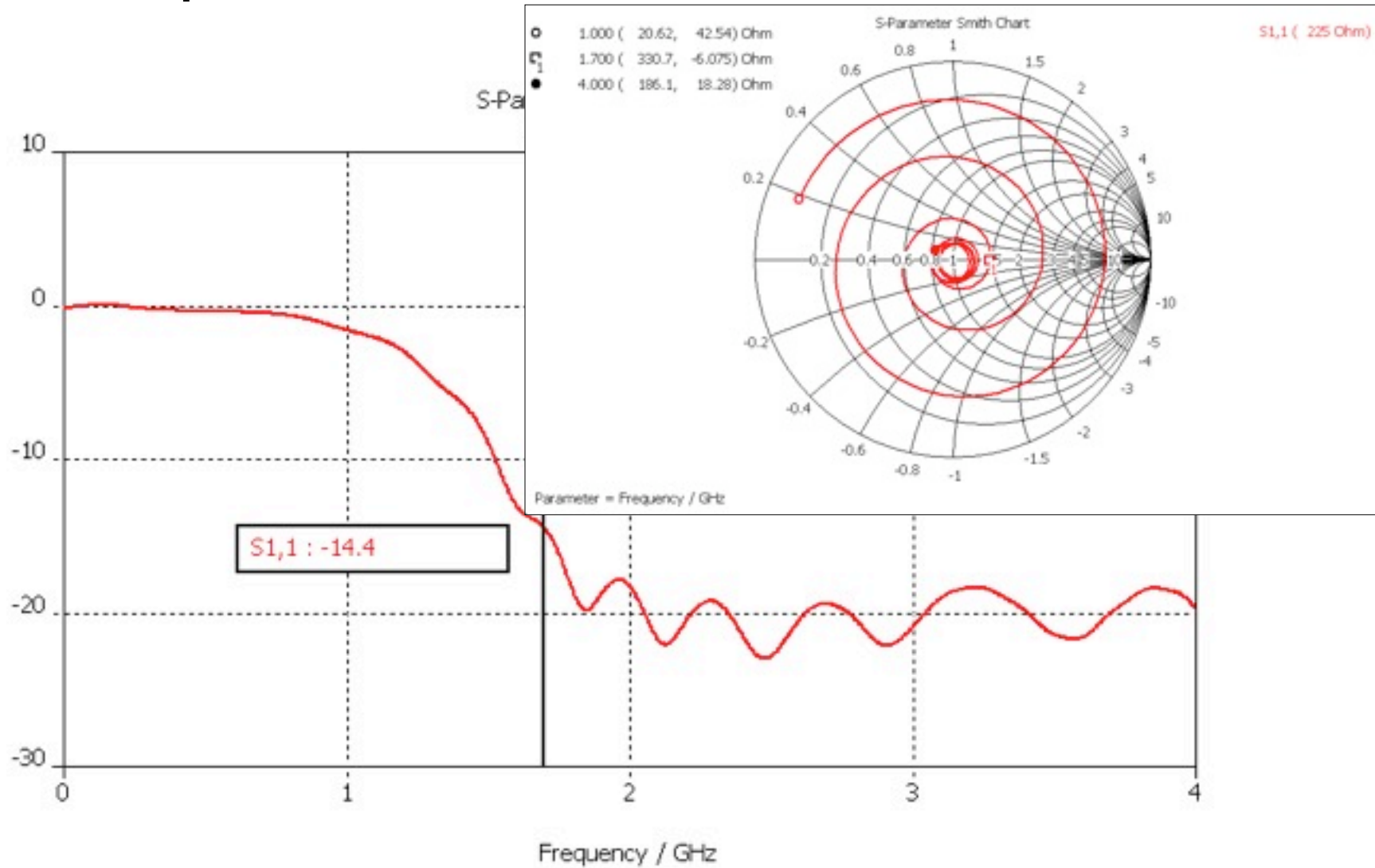


- Inexpensive photolithographic printing
- $>20$  dB rear rejection w/ no ground plane

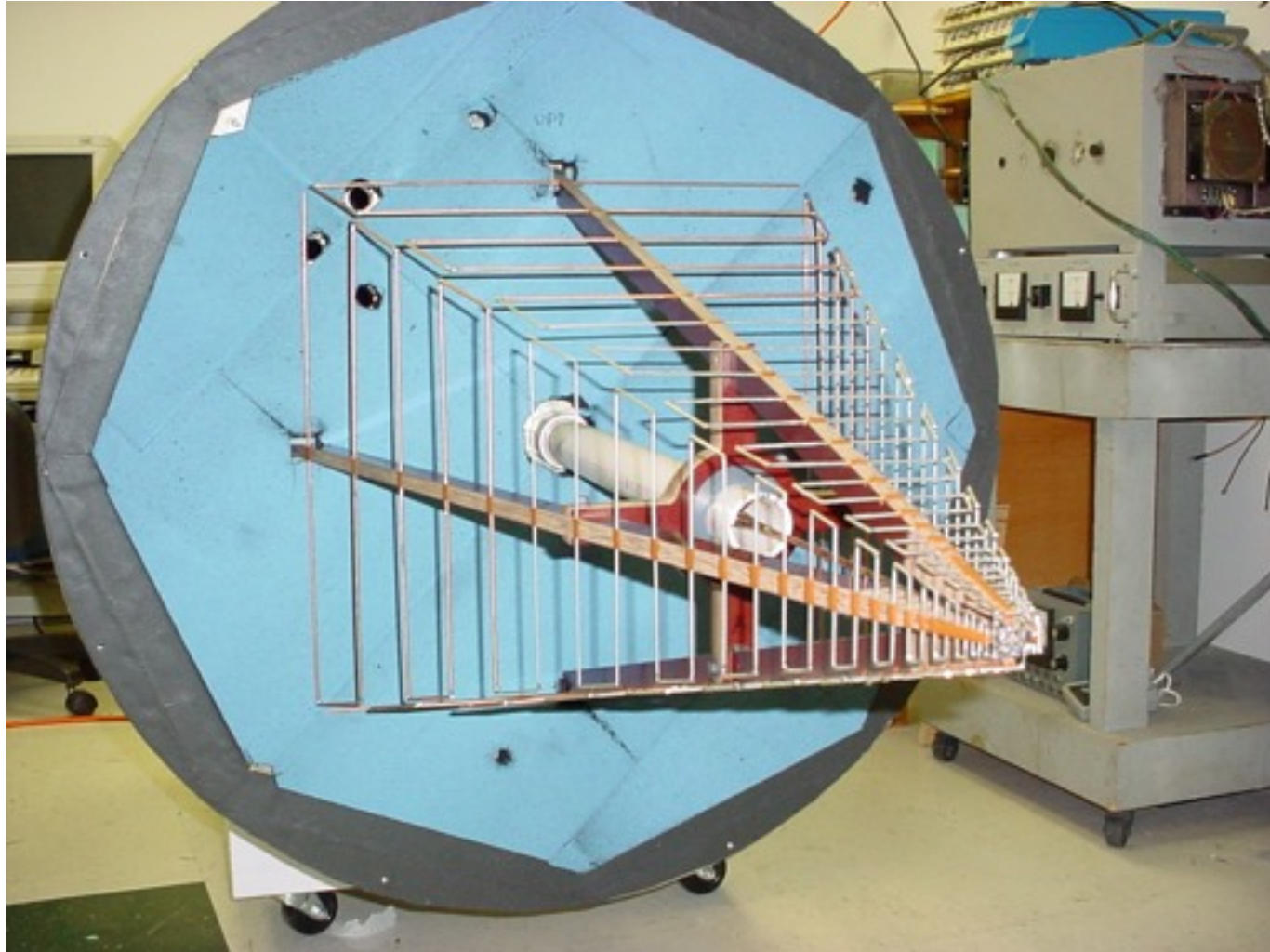
# Example return loss for 2-4 GHz case



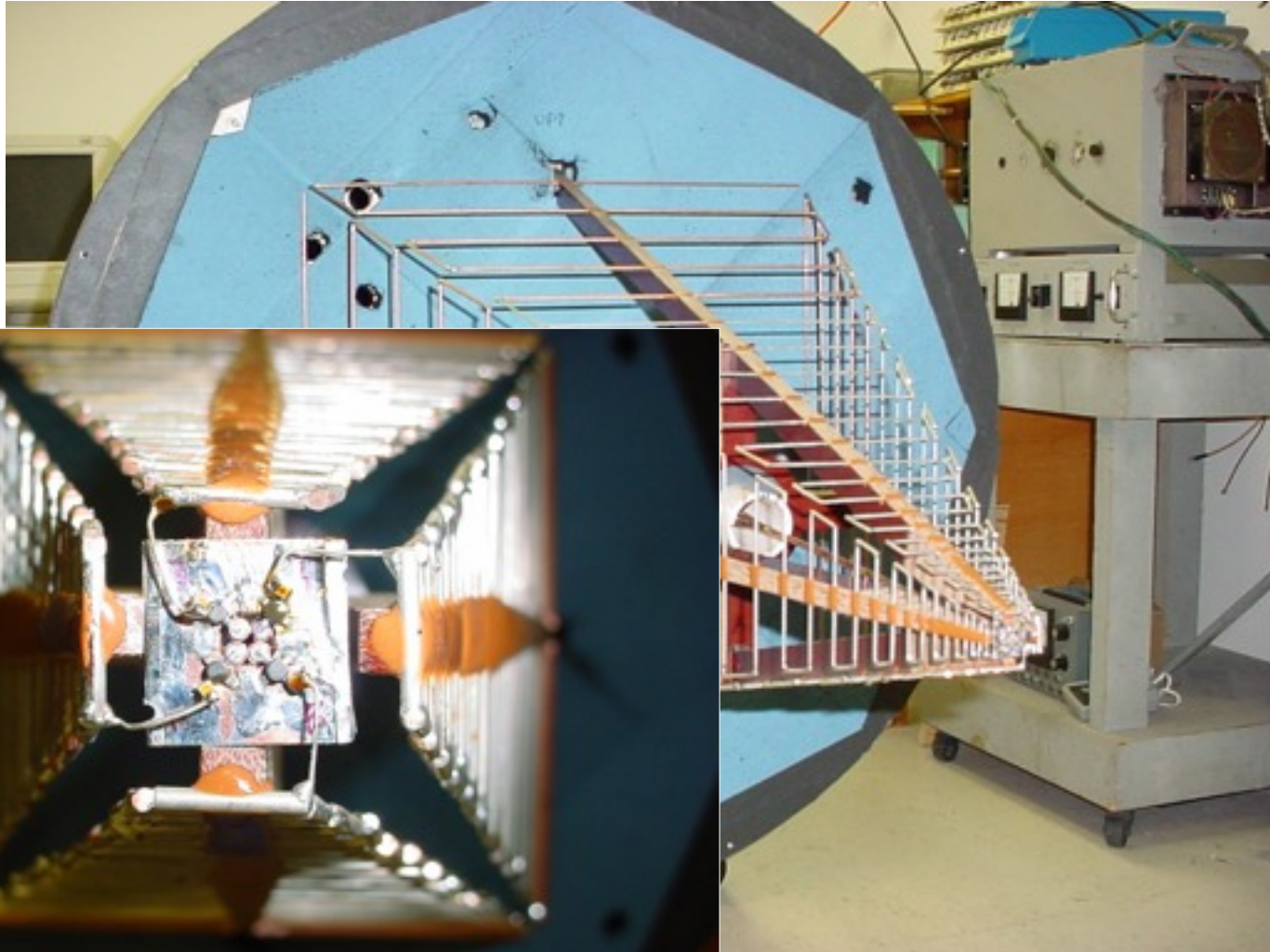
# Example return loss for 2-4 GHz case



# Trapezoidal-tooth pyramidal-type



# Trapezoidal-tooth pyramidal-type

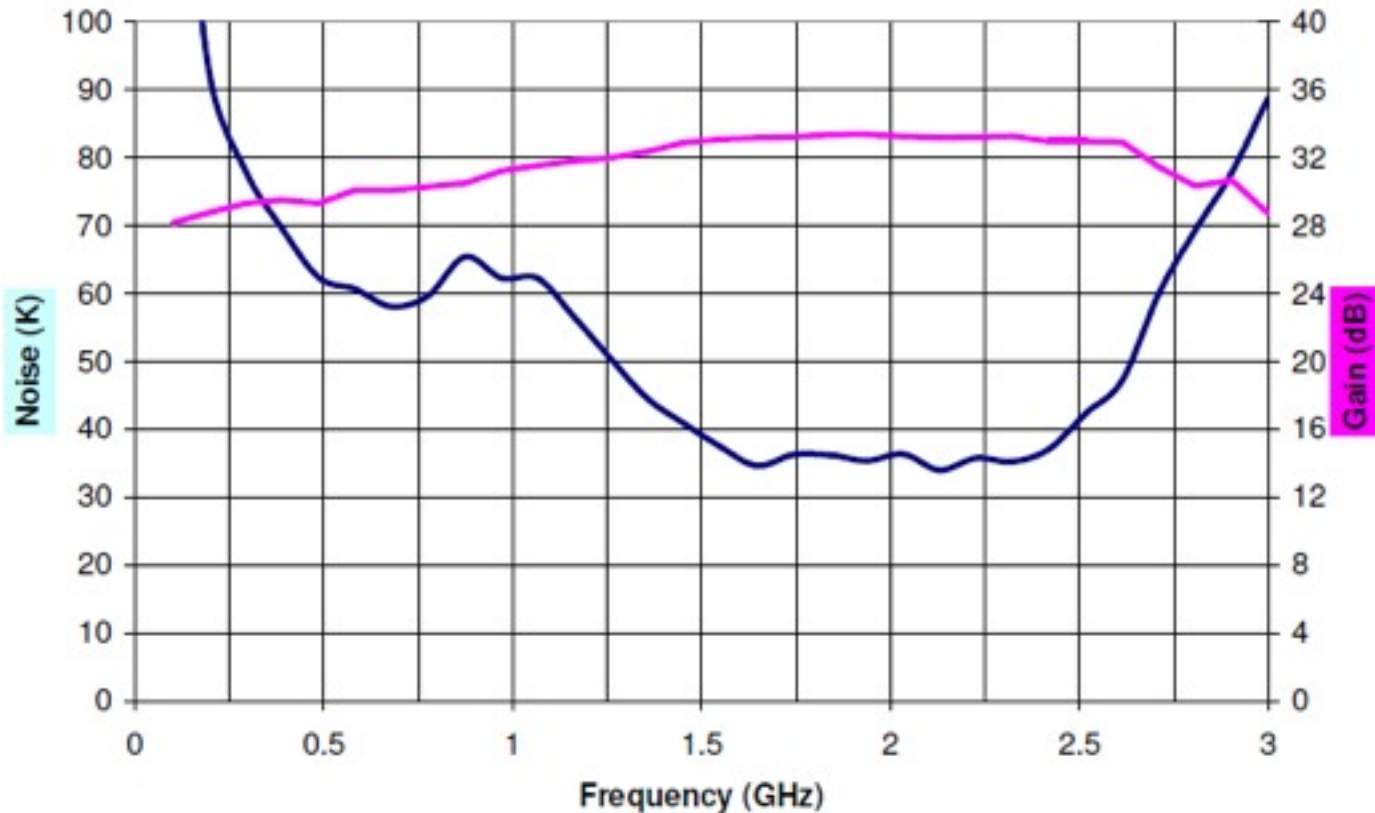


# Green Bank Solar Radio Burst Spectrometer

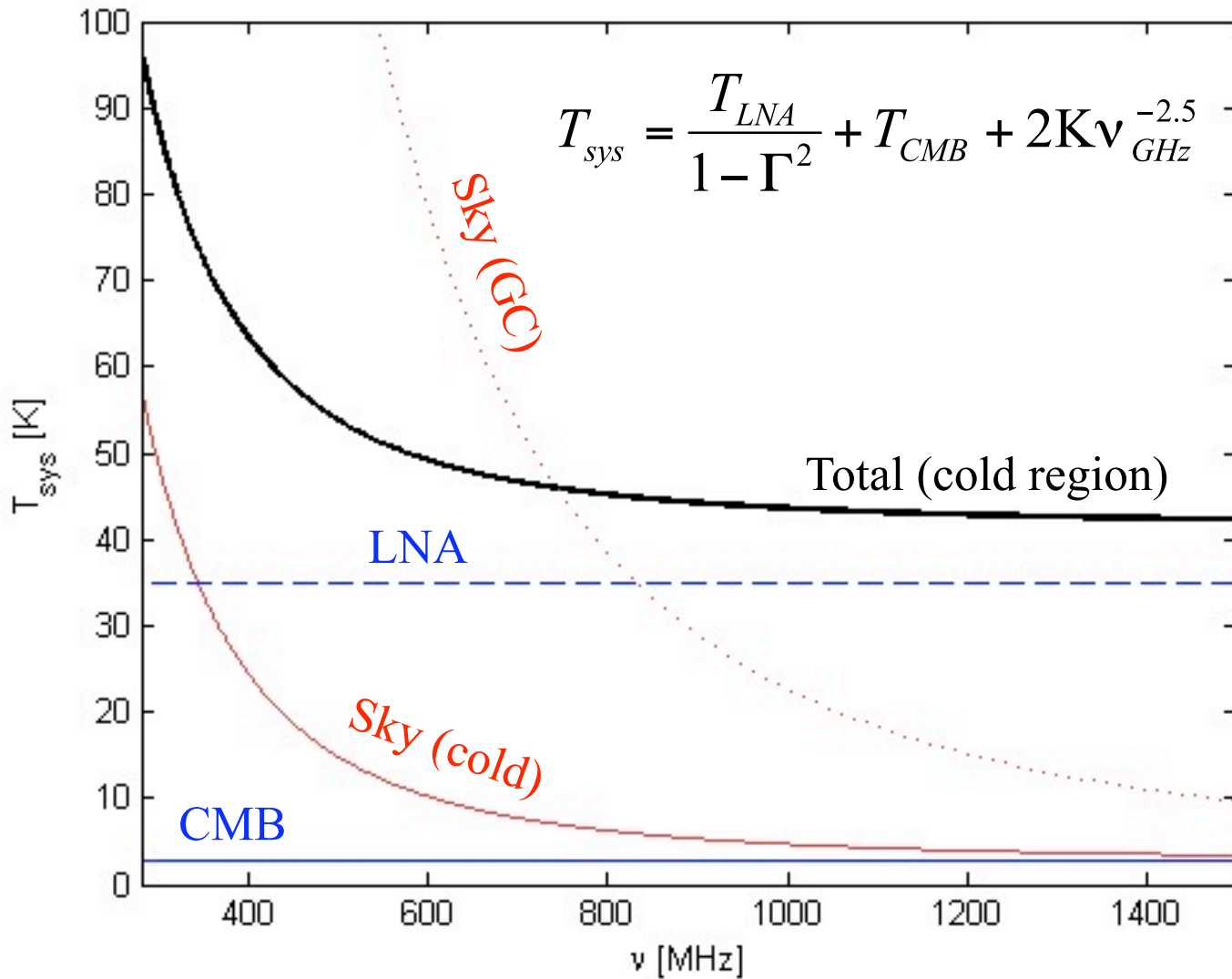


# HEFT LNA noise (unmatched)

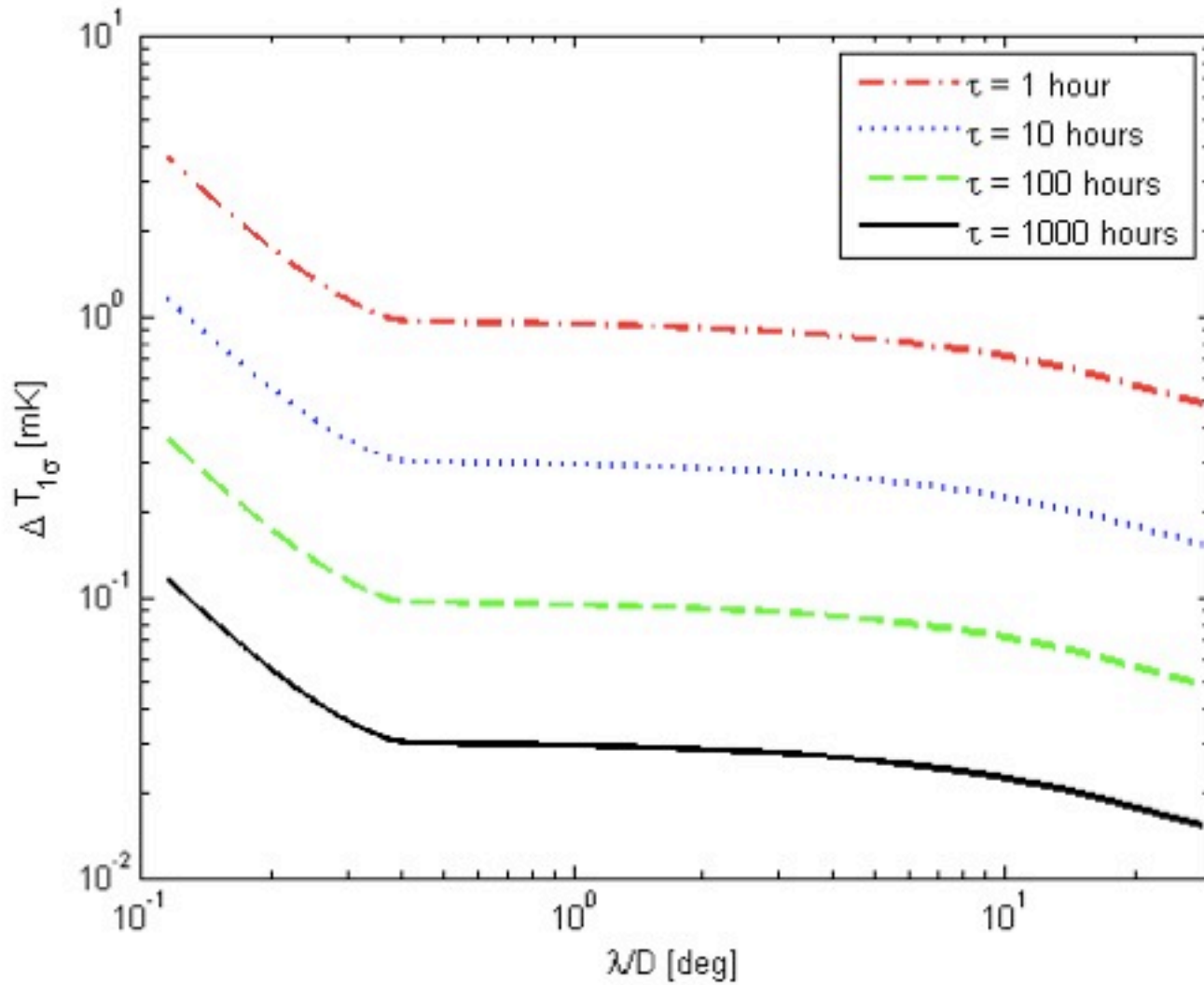
Two Stage LNA: FHX45X,  $V_d=1V$ ,  $I_d=20mA$



# System temperature

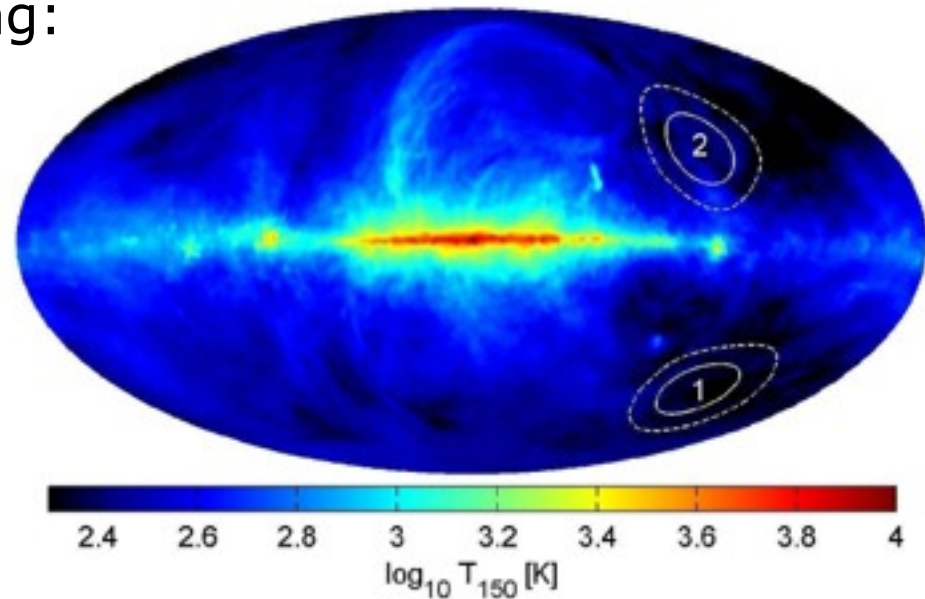


# Imaging sensitivity v. angular scale



# Observing strategy

- 3 fields, 1000-2000 hours each
- Tracking more efficient than drifting:
  - SNR 2x lower for same time
  - Not sample variance limited until >1000 hours, then only on largest scales



# Estimated uncertainty

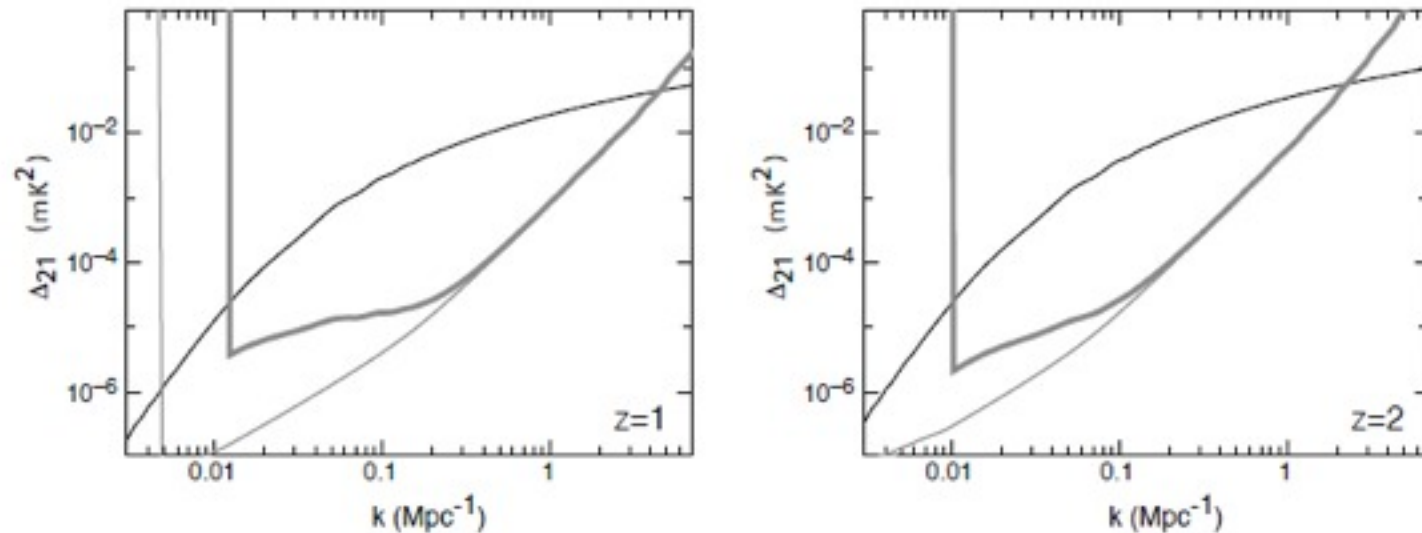


Figure 2: Examples of the post-reionization 21cm PS at redshifts 1 (left) and 2 (right). A DLA host mass of  $M_{(b)} = 10^{11} M_{\odot}$  was assumed at each redshift. The thick light curve shows the spherically averaged noise for the RCT, assuming 1000hr integration on each of three fields. The sharp upturn at low  $k$  is due to the assumption that foreground removal prevents measurement of the PS at scales corresponding to a bandpass larger than 80MHz. The cosmic variance (including the Poisson noise) component is plotted as the thin light curve. The sensitivity curves are plotted within bins of width  $\Delta k = k/10$ .

# Cosmology parameter estimation

Table 1:  $1\sigma$  Errors on cosmological parameters measured with the Radio Cosmology Telescope, following Visbal et al. (2008). We assume that 3 fields of view are imaged over the frequency range corresponding to  $z=1.2-4.0$  (280–640 MHz) and each frequency band within the field of view has been integrated for 2000 hours. Additional model parameters include a neutrino hierarchy with one dominant species having a neutrino mass of 0.05eV and a parameterization of the neutral hydrogen density to linear order,  $x_{\text{HI}} = x_{\text{HI1}} + x_{\text{HI2}}(z - z_{\text{center}})$ .

	$\Omega_{\Lambda}$	$\Omega_{\text{m}} h^2$	$\Omega_{\text{b}} h^2$	$n_{\text{s}}$	$A_{\text{s}}^2 \times 10^{10}$	$\alpha$	$\Omega_{\nu} h^2$	$w$
Fiducial Values	0.7	0.147	0.023	0.95	25.0	0.0	0.00054	-1
RCT	0.015	0.013	0.0032	0.027	–	0.012	0.0024	0.087
Planck	0.096	0.0061	0.00024	0.0094	0.27	0.0071	0.0059	0.16
RCT+Planck	0.01	0.00079	0.00018	0.0055	0.22	0.0042	0.00089	0.048

# Roadmap

2010-2011:

- Full antenna simulation
- MOFF FPGA prototype implementation
- Prototype antenna tile
- Detailed design and cost

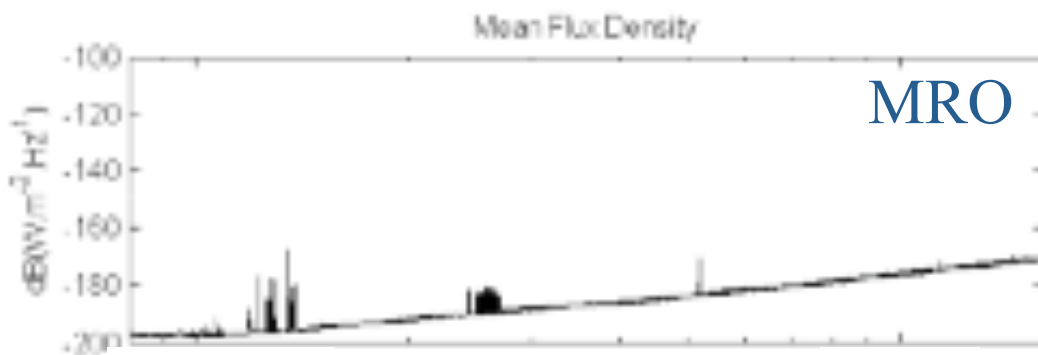
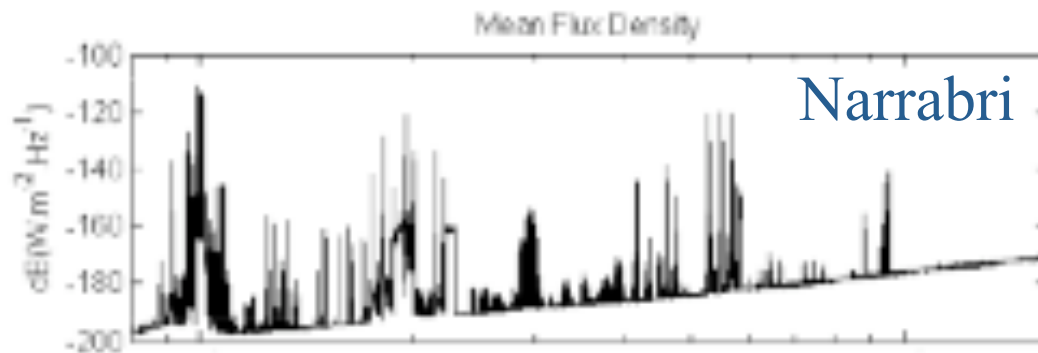
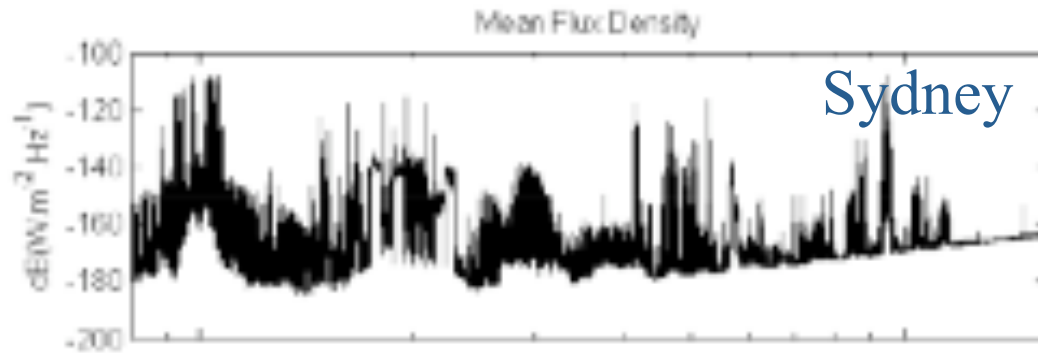
2012-2013:

- End-to-end demonstration

Looking for a mid-Decade start

# Site selection

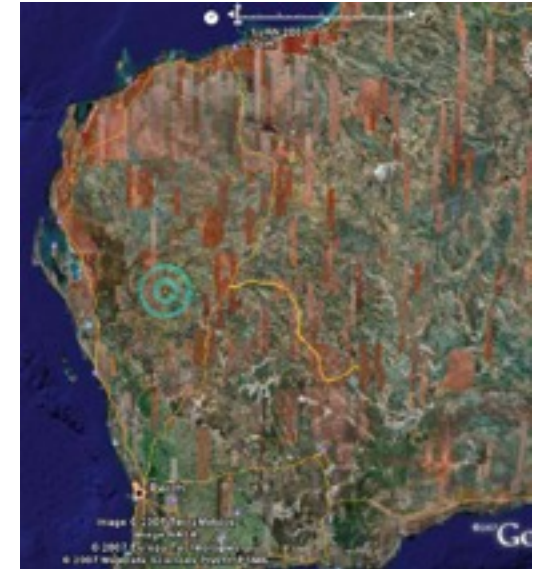
# CARPE reference site



100 MHz

1 GHz

Frequency [Hz]



# New England radio interference

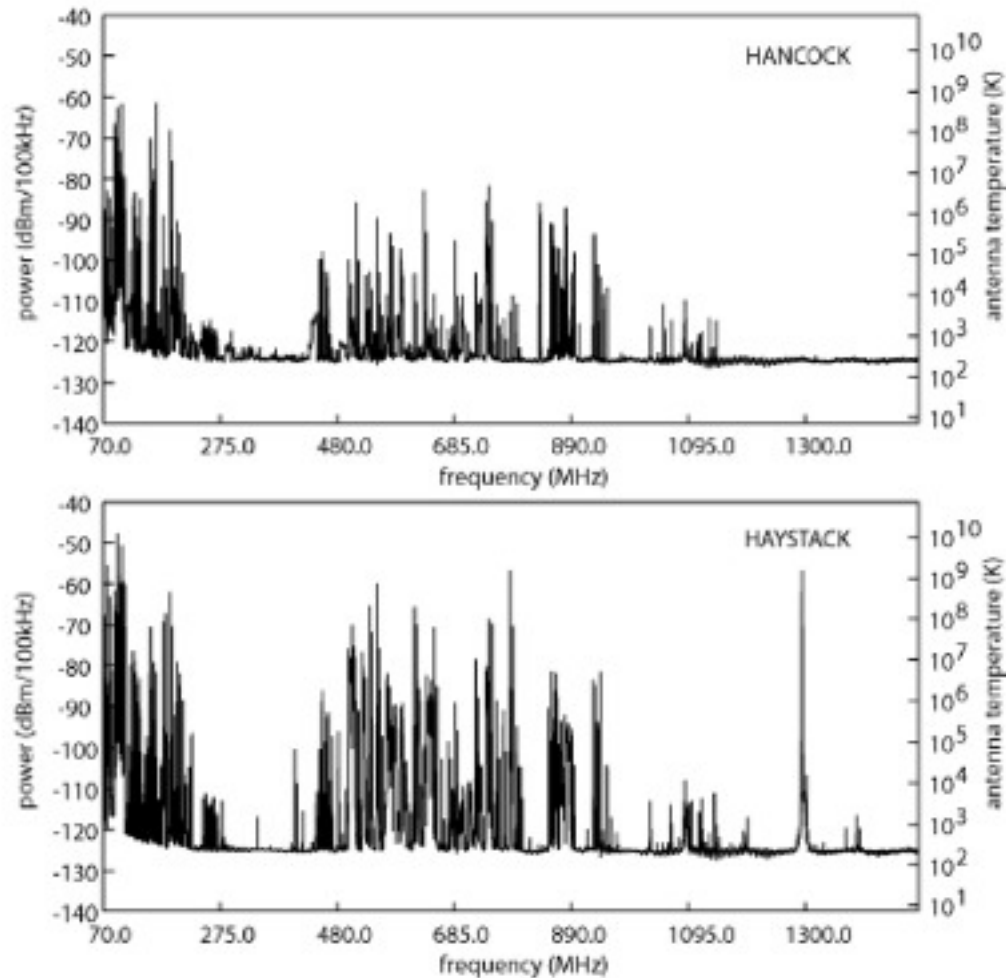
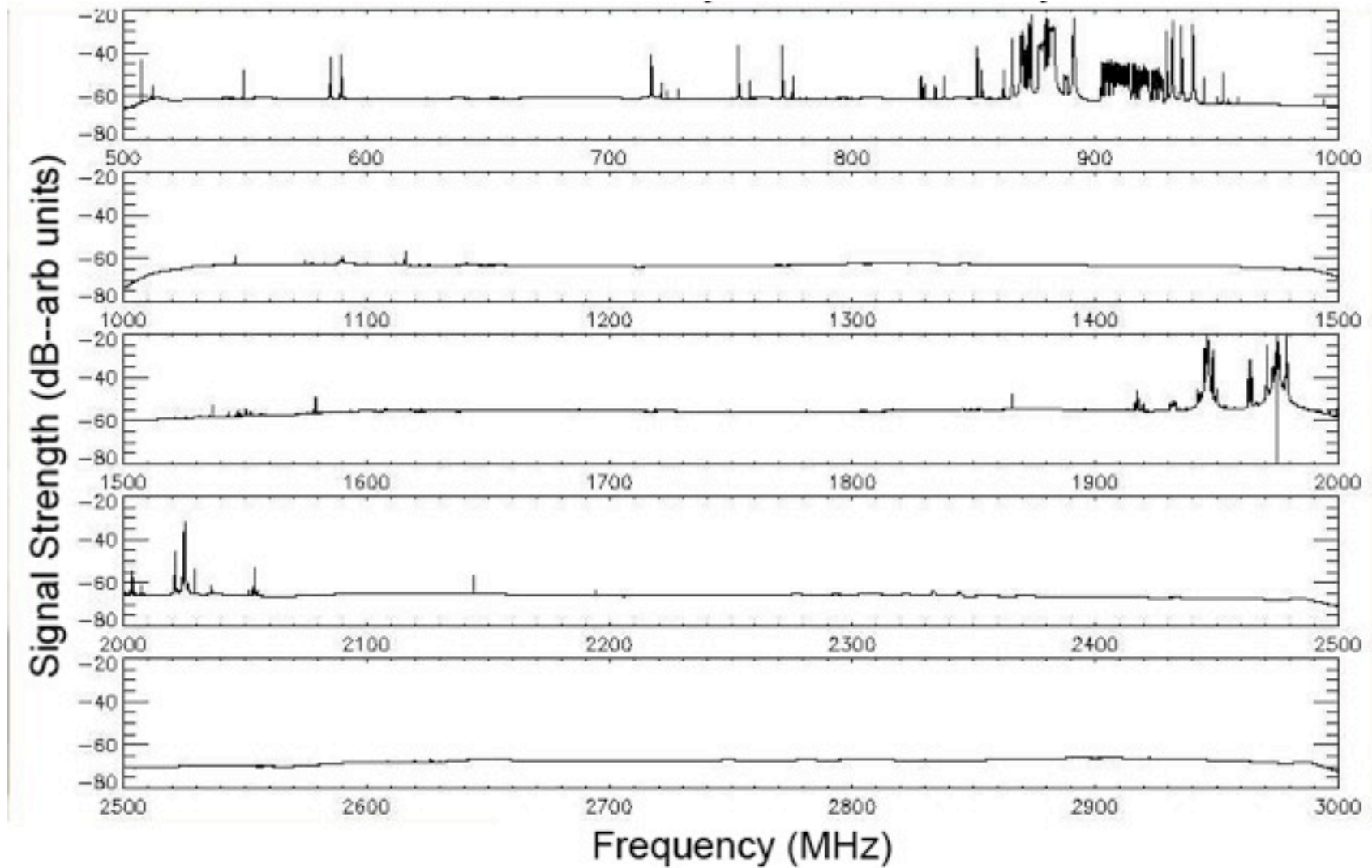


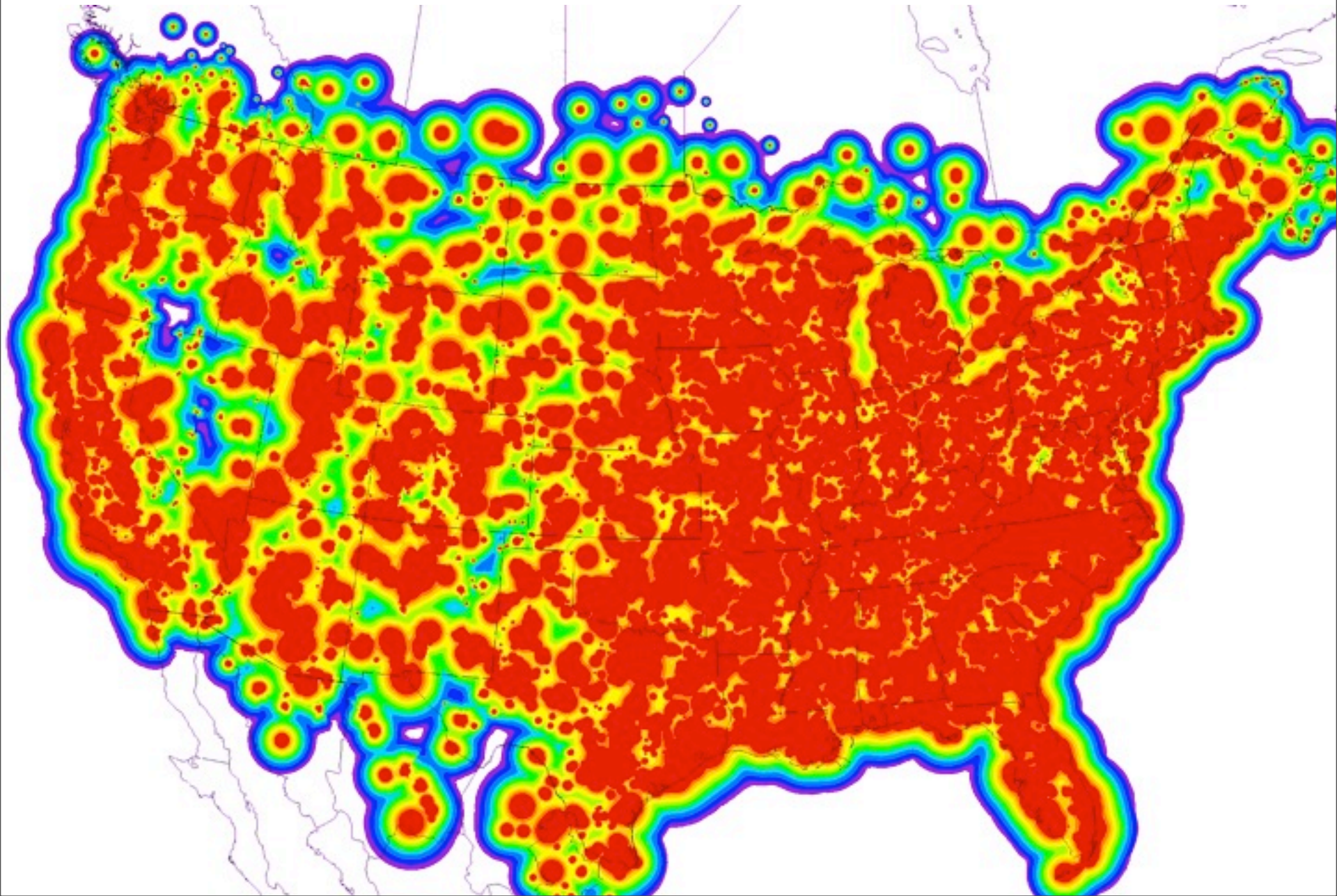
Fig. 2 Calibrated spectra from the Haystack site, and the Hancock site. The resolution is 100 kHz. The strong signal at 1295 MHz in the Haystack spectrum is from the adjacent Millstone radar, and the signals at approximately 1195 and 1395 are intermodulation products between the FM band and the radar. These spectra are an average of 24 hours.

# Owens Valley radio interference



Dale Gary

# FM and TV Strength



Saturday, October 10, 2009

# A bit more on foregrounds

# Foreground 2D power spectra

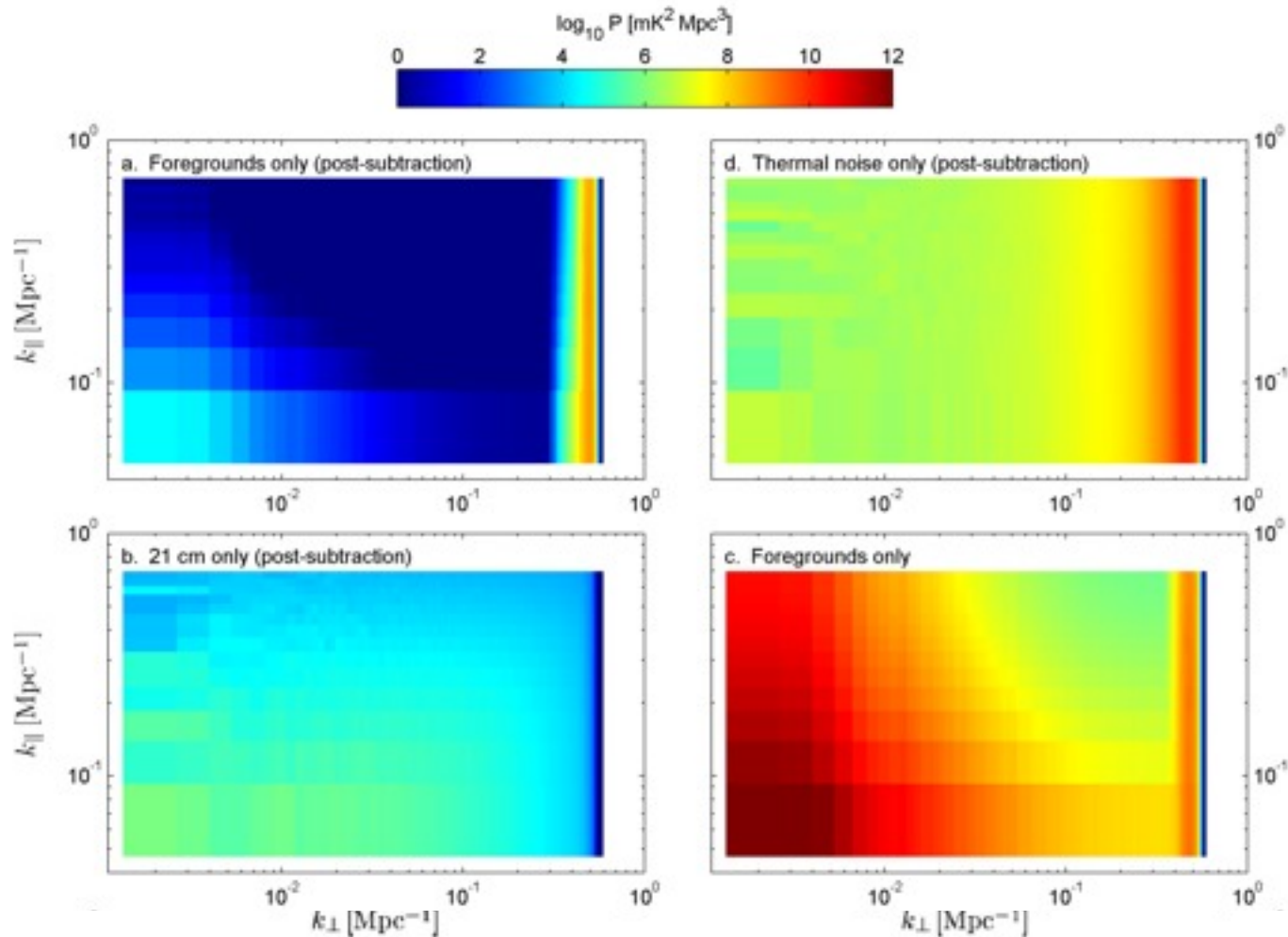


**Figure 11.** Two-dimensional power spectra of postsubtraction residuals from dirty maps generated with uniform weighting. For the left column of panels, the thermal noise has been artificially removed. It is evident that the foreground-only residuals following subtraction are much lower than the 21 cm signal in the range  $k_{\perp} \lesssim 3 \times 10^{-1}$ , beyond which corresponds to the outer annulus of poor foreground subtraction in the bottom panel of Figure 7. Panel (c) confirms that the 21 cm signal dominates the recovered power from the full-sky model since it appears nearly identical to panel (b). The white arcs in panel (f) illustrate the spherical shells of constant  $k$  that are used for the one-dimensional power spectrum in Figure 12.

# Foreground subtraction removes signal

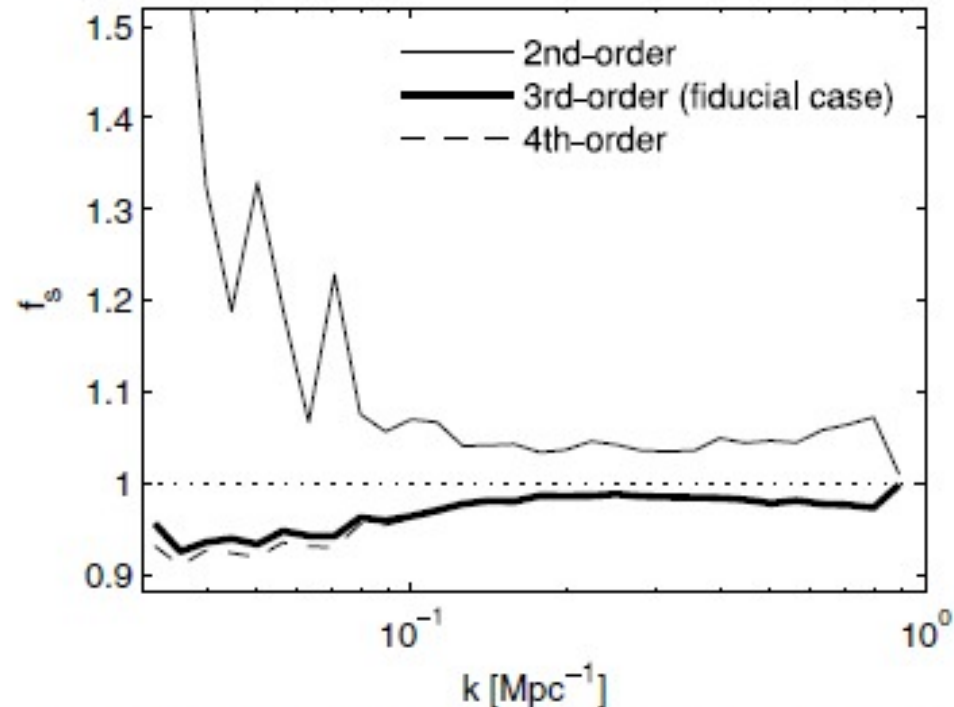


**Figure 13.** Subtraction characterization factor,  $f_s$ , for the one-dimensional binned power spectrum. The characterization factor is shown for three different levels of polynomial subtraction. As expected, the largest error is for large spatial modes (low  $k$ ). Over most scales, however, the correction for our fiducial third-order polynomial subtraction is only  $\sim 1\%$ .

# CARPE summary

- Large-N, small-D, high-dwell
- Complementary science goals: DE, Pulsars
- Leverage significant effort in reionization arrays to mitigate calibration and foreground risks
- Exploit new correlator and DSP capabilities